Title

Spatial distribution of damage potential of the 2023 Pazarcik Turkey earthquake using inelastic-response spectra of recorded and simulated ground motions

Journal

Earthquake Spectra, 41(1)

ISSN

8755-2930

Authors

Zengin, Esra
Bozorgnia, Yousef
Tamhidi, Aidin
et al.

Publication Date

2025-02-01

DOI

10.1177/87552930241270609

Journal of Earthquake Engineering

ISSN: (Print) (Online) Journal homepage: www.tandfonline.com/journals/ueqe20

Evaluation of the Impacts of Different Ground Motion Selection and Scaling Approaches on Seismic Performance of Bridges

Esra Zengin, Saiid Saiidi & Yousef Bozorgnia

To cite this article: Esra Zengin, Saiid Saiidi & Yousef Bozorgnia (2025) Evaluation of the Impacts of Different Ground Motion Selection and Scaling Approaches on Seismic Performance of Bridges, Journal of Earthquake Engineering, 29:4, 938-956, DOI: 10.1080/13632469.2025.2458598

To link to this article: https://doi.org/10.1080/13632469.2025.2458598

JOURNAL OF EARTHQUAKE ENGINEERING
2025, VOL. 29, NO. 4, 938–956
https://doi.org/10.1080/13632469.2025.2458598

Taylor & Francis
Taylor & Francis Group

Evaluation of the Impacts of Different Ground Motion Selection and Scaling Approaches on Seismic Performance of Bridges

Esra Zengin, Saiid Saiidi, and Yousef Bozorgnia

Natural Hazards Risk and Resiliency Research Center (NHR3), University of California, Los Angeles (UCLA), Los Angeles, California, USA

ABSTRACT

This paper investigates two ground motion selection and scaling (GMSS) methods for assessing the seismic performance of bridges in high seismic regions in California. It compares the traditional GMSS approach using elastic probabilistic seismic hazard analysis (PSHA) with a novel method based on inelastic PSHA, scaling ground motions to spectra across varying ductility levels. Nonlinear response history analyses of a 3-span bridge using 25 ground motions show that the inelastic PSHA-based method can reduce dispersion in responses, increasing confidence in seismic performance estimates. The traditional approach may produce conservative or unconservative results due to mismatches between scaled and target spectra.

ARTICLE HISTORY
Received 20 September 2024
Accepted 19 January 2025

KEYWORDS
Bridge response; ground motion selection and scaling; inelastic PSHA; ductility; seismic performance; residual drift ratio

1. Introduction

Ensuring the safety and resilience of the bridges requires a thorough understanding of their seismic performance, which can be reached by nonlinear response history analysis (NRHA) utilizing a set of ground motions compatible with a target spectrum across a specified period range. In traditional ground motion selection and scaling (GMSS) approaches, the ground motions are typically selected based on general parameters of the controlling scenario event, such as magnitude, source-to-site distance, and site characteristics. In the "amplitude scaling" approach, the spectral ordinates of the selected ground motions are scaled using constant factors. The efficacy of the GMSS approaches shapes the behavior of the fragility curves and impacts seismic risk assessments of structures.

Commonly used GMSS methods often utilize the relatively conservative Uniform Hazard Spectrum (UHS) as the target spectrum, derived from probabilistic seismic hazard analysis (PSHA) based on the elastic response of a single-degree-of-freedom (SDOF) oscillator. To address the inherent conservatism of the UHS, an alternative, the Conditional Mean Spectrum (CMS), has been proposed for seismic performance assessment and record selection (Baker 2011). As an improvement over CMS, the Conditional Spectrum (CS), which considers the aleatory variability of ground motions, has been suggested to provide a more comprehensive perspective on seismic risk assessment (Jayaram, Lin, and Baker 2011). While most GMSS approaches use elastic spectral ordinates as the intensity measure (IM), alternative IMs like peak ground motion parameters and damage indices have been investigated. Monteiro et al. (2019) demonstrated that the Fajfar index (Iv), peak ground velocity (PGV), and root mean square velocity (vRMS) yield lower dispersion across fitted fragility curves for a population of bridges. Some studies have developed GMSS approaches incorporating advanced scalar and vector IMs (Kohrangi, Bazzurro, and Vamvatsikos 2016; Tarbali, Bradley, and Baker 2019; Zengin 2022; Zengin and Abrahamson 2020a, 2020b; Zengin and Abrahamson 2021). Bradley (2010) introduced a generalized conditional intensity measure (GCIM) approach explicitly considering various IMs

CONTACT Esra Zengin esrazengin@g.ucla.edu Natural Hazards Risk and Resiliency Research Center (NHR3), University of California, Los Angeles (UCLA), Los Angeles, CA 90095, USA

beyond spectral accelerations, including cumulative absolute velocity, Arias Intensity, and significant durations. Recently, Bahrampouri et al. (2023) proposed a methodology to incorporate the inelastic response of an SDOF oscillator in PSHA, addressing limitations associated with relying solely on elastic responses. This approach adopted a constant ductility inelastic spectrum, where the seismic coefficient (Cy) corresponding to the ratio of the yield strength (Fy) to weight (W) of an inelastic SDOF oscillator matches with the specific displacement ductility demand (μ) (i.e. the ratio of the maximum displacement of the inelastic SDOF oscillator to the yield displacement) induced by ground motions. In this context, the effects of yielding, plastic deformation, and hysteretic energy dissipation were considered, leading to a more realistic yet simple representation of the inelastic behavior of the structure. The inelastic PSHA was performed using the ground-motion models (GMMs) specifically developed for inelastic SDOF systems. Bahrampouri et al. (2023) proposed an amplitude-scaling GMSS method that adjusts ground motions to be compatible with both elastic and inelastic spectra across different μ levels. Their approach also controls the variability of the selected motions with a specified target standard deviation.

This study investigates how traditional elastic PSHA-based and novel inelastic PSHA-based GMSS approaches influence the seismic performance of a three-span bridge designed according to Caltrans Seismic Design Criteria (SDC 2019). By analyzing a modified Arroyo de la Laguna bridge across sites with varying seismicity, i.e. Los Angeles, San Francisco, and San Bernardino, this study examines the impact of different GMSS approaches and target spectra definitions on key structural performance metrics, such as column drift ratios, as well as on damage states, fragility curves, and drift hazard curves. Additionally, the study investigates the effects of pulse characteristics on residual drift ratios, offering insights into how these characteristics can impact the seismic response of the bridge and its long-term safety following seismic events.

2. Probabilistic Seismic Hazard Analysis of the Sites

Site-specific elastic and inelastic PSHA for ten California sites, assuming rock conditions with a shear wave velocity of Vs_{30} = 760 m/s, were conducted by Bahrampouri et al. (2023). The elastic GMM used was NGA-West2 Campbell and Bozorgnia (CB14) (Campbell and Bozorgnia 2014), while a new GMM for inelastic SDOF systems was developed by Bahrampouri et al. (2023). Utilizing the new inelastic GMM and UCERF3 (Field et al. 2014) seismic sources, PSHA was performed for inelastic Cy spectra at each site. Among the ten sites, Zengin, Saiidi, and Bozorgnia (2023) selected five sites based on their 5% damped pseudo-spectral acceleration (PSA) levels, considering the PSA ratio (for T_R = 2475 years divided by that for T_R = 975 years). Here, the target period was set at 1.0 second, corresponding to the transverse period of the bridge model used in this study. The seismicity ranking of sites, determined by T_R = 975 years (i.e. 5% probability of exceedance in 50 years), indicated the following order: San Bernardino had the highest seismic hazard, followed by Oakland, Los Angeles, San Francisco, and Long Beach. For brevity, the part of the study presented in this article focuses on findings from three representative sites from the list of five: Los Angeles, San Francisco, and San Bernardino. Comprehensive details can be found in the study by Zengin, Saiidi, and Bozorgnia (2023). The target spectra, i.e. CMS and UHS, were computed for five return periods (T_R = 200, 475, 975, 2475, and 5000 years). Different sets of ground motion were selected and amplitude-scaled to "match" the target spectra at the five T_R levels, as discussed in the subsequent section. Table 1 provides the PSA (T = 1.0 s)

Table 1. Target PSA (T = 1.0 s) [g] corresponding to each T_R for each site.

Return Period (T_R) (years)	Los Angeles	San Francisco	San Bernardino
200	0.17	0.17	0.24
475	0.28	0.26	0.40
975	0.41	0.35	0.56
2475	0.61	0.50	0.81
5000	0.80	0.62	1.03

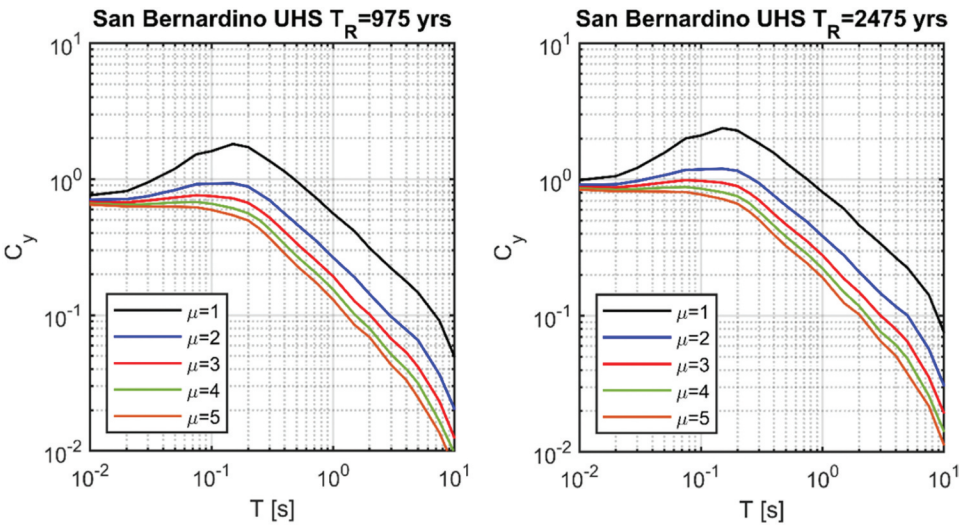

Figure 1. UHS of inelastic C_y for different μ levels at two T_R levels for San Bernardino.

values, representing elastic target IM levels for each return period. When comparing high and low seismicity sites, specifically San Bernardino and San Francisco, it is observed that the PSA ($T = 1.0$ s) for San Bernardino at $T_R = 975$ years is approximately 1.6 times higher than that of San Francisco. This UHS corresponds to the design spectrum for Safety Evaluation Earthquake (SEE) as per the Caltrans SDC.

Figure 1 illustrates the UHS for inelastic Cy at various ductility μ levels for San Bernardino at two T_R levels. In this case, Cy(for μ = 1) represented the seismic coefficient required to prevent structural yielding (i.e. elastic behavior), whereas Cy(for μ=μi) corresponded to the ordinate values on a constant-ductility inelastic spectrum, matching the target ductility μi. As expected, Cy demand decreases with increasing μ (e.g. Bozorgnia and Bertero 2004; Bozorgnia, Hachem, and Campbell 2010; Zengin et al. 2024). These spectra served as the targets for the GMSS approach utilizing inelastic PSHA results, as detailed in the subsequent section.

3. Ground Motion Selection and Scaling Approaches

In the analysis of inelastic SDOF oscillator responses a subset of 7203 ground motions from the NGA-West2 database was utilized (Bozorgnia et al. 2014; Mazzoni, Bozorgnia, and Bahrampouri 2023). The records were within the closest rupture distance (R_{rup}) of 80 km, which generally is important for engineering applications. The candidate database for ground motion selection was further constrained using the disaggregation results from PSHA. It was noted that the dominant scenario earthquake magnitude (M) and R_{rup} values varied with T_R levels, ranging from M 6.5 to M 8.0 and 0 to 20 km, respectively. To achieve better fits between the spectral shapes of the records and the target spectra, M ranging from 5.5 to 7.9 and R_{rup} from 0 to 40 km were considered, without imposing site class restrictions. The ground motions were limited to a maximum scale factor of 5.

The first amplitude-scaling GMSS approach employed in this study, referred to as elastic PSHA-based GMSS, scales ground motions to be compatible with the average spectrum of the target UHS or CMS derived from elastic PSHA. The second approach, called the inelastic PSHA-based GMSS, scales the ground motions to be compatible with multiple target spectra representing different ductility levels obtained from the inelastic PSHA. This approach can simultaneously match both the desired target mean and standard deviation for elastic and inelastic-PSHA-based spectra. It uses a method called the Kullback-Leibler Divergence (KLD) criterion to select ground motions that are compatible with the

target spectrum (Bahrampouri et al. 2023; Kullback and Leibler 1951). The KLD criterion quantifies information loss when approximating one distribution with another, avoiding subjective weighting and improving standard deviation handling compared to traditional methods. A greedy search algorithm was used to select ground motions, starting with those best matching the target mean and iteratively refining the selection based on a cost function.

Twenty-five ground motions were scaled to match their spectra with the target spectra over a period range of 0.4 to 4.0 seconds. The target standard deviation was set to one-half of the standard deviation (i.e. 0.5sigma) of the CB14 GMM to maintain consistent record-to-record variability (i.e. spectral variability) within the suite of ground motions. This approach aimed to achieve uniform spectral variability across different GMSS methods. A similar level of variability could be achieved based on the sum of squared errors (SSE) comparing the natural logarithmic spectral accelerations of the 25 ground motions with the elastic target spectrum, but SSE was not used.

Initially 20 ground motions were scaled using the RotD50 component (Boore 2010). Between the two horizontal components, the components that best matched the target spectrum were selected for the NRHA of the bridge model. It was assumed that the critical bridge responses could be captured by input motions that were applied in the transverse direction to simplify comparisons between GMSS methods, isolating the effects of record selection and scaling without the added complexity of bidirectional ground motions. There was no distinction between pulse-like and non-pulse-like records in the selection of the 20 ground motions as long as the spectral shape closely matched the target. It was observed that the subsets with T_R values less than 2475 years typically included only a few records with pulses (1 to 4). However, as the T_R values reached or exceeded 2475 years, the number of pulse records in these subsets increased significantly (3 to 10). The findings indicated that sites with high seismicity, such as San Bernardino, had more pulse records, and their pulse period (T_p) values were generally greater than $3T_1$. In addition to the 20 ground motions selected using different GMSS approaches, a separate subset of 5 records was explicitly chosen from a pool of pulses T_p ranging from 0.5 to 2.0 seconds (Shahi and Baker 2014), based on SSE criteria to ensure the inclusion of at least five records with pulse characteristics that may influence the bridge's response.

Figure 2 illustrates a suite of motions selected and scaled using both the traditional elastic PSHA-based GMSS approach (left panel) and the inelastic PSHA-based GMSS approach (right panel) for UHS as the target at $T_R = 975$ years for Los Angeles. Here, the differences between the means and

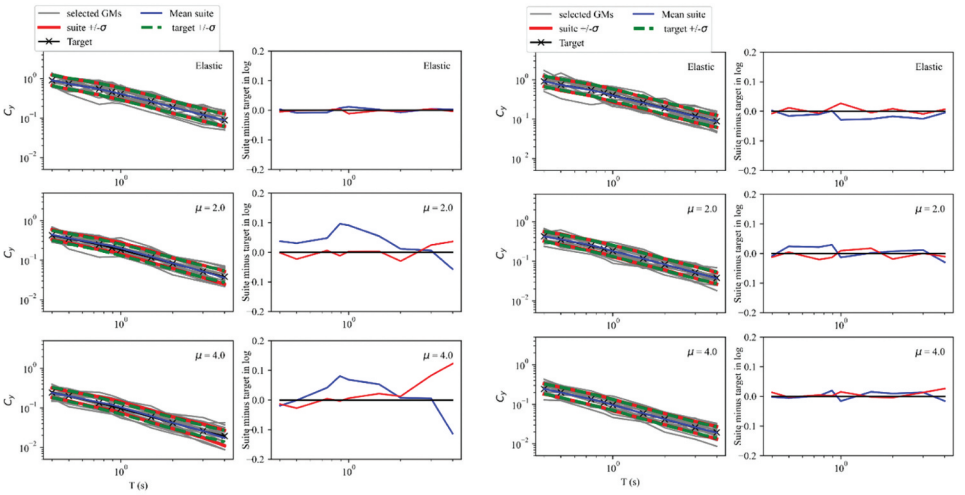

Figure 2. Comparisons of the spectra of the suite mean and standard deviation with the targets for elastic and inelastic **UHS** representing different displacement ductility levels, at $T_R = 975$ years, for Los Angeles, using the elastic PSHA-based GMSS approach (left panel), and the inelastic PSHA-based GMSS approach (right panel).

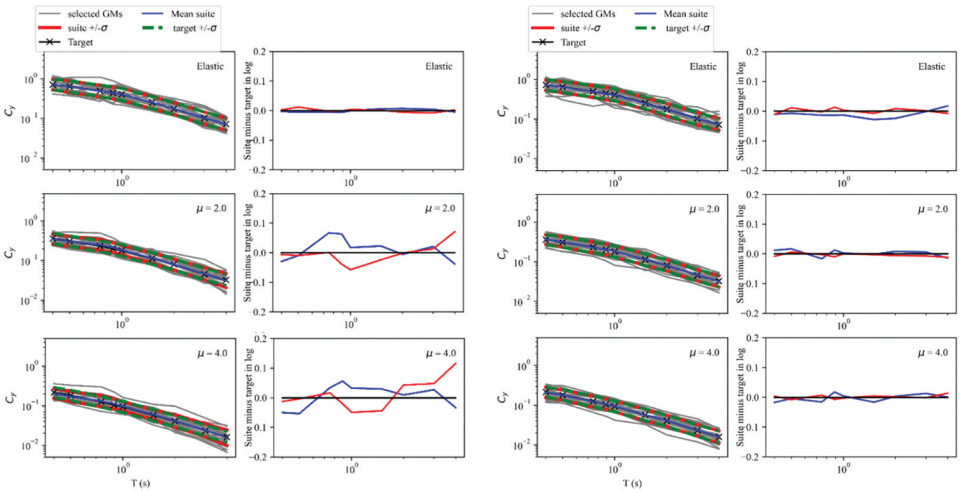

Figure 3. Comparisons of the spectra of the suite mean and standard deviation with the targets for elastic and inelastic **CMS** representing different displacement ductility levels, at $T_R = 975$ years, for Los Angeles, using the elastic PSHA-based GMSS approach (left panel), and the inelastic PSHA-based GMSS approach (right panel).

standard deviations (i.e. error) were calculated as the difference between the suite and target mean (and standard deviation, σ) in natural log units. These errors are plotted alongside the spectra. While the elastic PSHA-based GMSS approach aimed for compatibility between elastic record spectra and target spectra, the inelastic response spectra of the scaled records were also compared with the inelastic UHS targets at different μ levels (ranging from 1 to 5) to evaluate the extent of mismatches with the inelastic targets. The results indicated that the elastic PSHA-based GMSS approach resulted in a good match with the elastic target spectrum; however, generally it tended to overestimate the target mean inelastic spectra at various μ levels and failed to accurately capture the target σ especially at long periods. The inelastic spectra are shown at μ = 2 and 4. Error trends at μ = 3 and 5 were similar but not included for brevity. As seen, the inelastic PSHA-based ground motions demonstrated a very good agreement with both the target mean and standard deviation across multiple response spectra, showing greater consistency.

Figure 3 presents the comparisons for the target CMS cases with a conditioning period of 1.0 second. It was observed that the elastic PSHA-based GMSS approach slightly overestimated the target mean of the inelastic response spectrum at high μ levels and poorly captured the target standard deviation over the specified period range. On the other hand, the inelastic-based GMSS for CMS showed good agreement with the target means and standard deviations. It was noted that depending on the target hazard level and constraints imposed in the GMSS process, the elastic CMS-based approach yielded either comparable or overestimated results compared to the inelastic approach. Detailed comparisons for elastic and inelastic PSHA-based GMSS approaches for each site, T_R level, and target spectrum can be found in Zengin, Saiidi, and Bozorgnia (2023).

4. Bridge Description and Three-Dimensional Model

The structural drawings of the Arroyo de la Laguna bridge were used as the basis of the bridge model studied herein. The bridge comprises three spans (90 ft side spans, 130 ft middle span). The bridge superstructure includes six California Wide Flange girders (CA WF60) with a total width of 64 ft. Piers consist of three 60“diameter columns connected to 24” diameter Cast-in-Drilled-Hole (CIDH) piles. The skewed abutment at 40° has a seat-type design supported by 30” diameter CIDH piles. This study employed several assumptions to maintain the broad applicability of the model and avoid introducing

details that would make the analysis overly specific to a particular bridge category. These assumptions were made to ensure that the focus remained on assessing the effects of GMSS methods on structural responses, rather than on variations in structural parameters. The structure was assumed to be cast-in-place with integral bent caps. A zero skew angle was assumed, as investigating the effect of skew angle on GMSS approaches for bridges was beyond the scope of this study. Column base details were assumed as two-way hinges allowing unrestrained rotational movement in two principal directions, acting as "pins." Such "pin" details are commonly used in the column bases of many California bridges to reduce foundation costs. Figure 4 illustrates elevation and plan views of the modified bridge model, along with girder cross-sections, column, and hinge cross-sections. It is important to note that the column height and cross section in the bridge model were adjusted to achieve a transverse period of 1.0 second.

The columns in Ordinary Standard Bridges (OSB) are classified as Seismic Critical Members (SCMs) where plastic hinge mechanisms take place, whereas the decks, girders, and cap beams are designated as capacity-protected (CP) members that behave elastically even during column plastic deformation (SDC 2019). In this study, the nonlinear behavior of the bridge was simulated through a three-dimensional (3D) model developed using the OpenSees software (Mazzoni et al. 2006; McKenna, Scott, and Fenves 2010). For columns, fiber-section Euler-Bernoulli force-based beam-

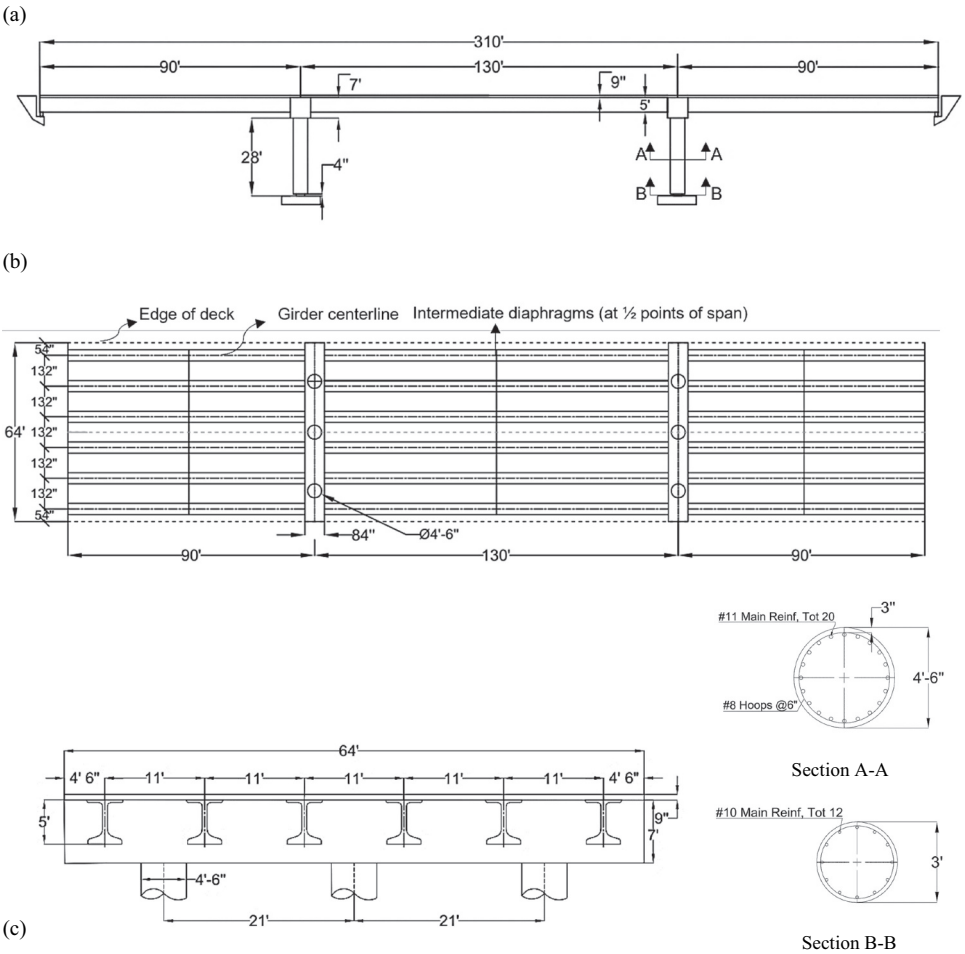

Figure 4. (a) Elevation view of the bridge model (b) Plan view of the bridge model (c) Cross sections of the girder, column and hinge.

column elements with distributed plasticity (*forceBeamColumn*) were utilized. These elements account for the interaction between axial force and bending moment at the section level, and numerical evaluations were performed at five Gauss-Lobatto integration points distributed along the length of the column (Neuenhofer and Filippou 1998; Scott and Hamutçuoğlu 2008). Concrete02 (Yassin 1994) and Steel02 (Menegotto and Pinto 1973) uniaxial material models were employed, with the stress-strain relationship for confined concrete based on the theoretical model by Mander, Priestley, and Park (1988), neglecting the tensile strength of the concrete. Parameters defining the stress-strain behavior can be found in Zengin, Saiidi, and Bozorgnia (2023). Torsional stiffness in the column fiber section was considered by assigning it to the backbone curve using the Eqs. $0.2 \times G_{conc}$ x J_{col}, where G_{conc} represents the shear modulus of concrete, and J_{col} denotes the polar moment of inertia. The torsional stiffness was reduced by 80% to account for the cracking of the column cross-section cracking (Aviram, Mackie, and Stojadinovic 2008; Shoushtari et al. 2021). The P-delta effect was incorporated into the bridge model to consider the interaction between axial loads and lateral deflection. For the superstructure of the bridge, elastic beam-column elements (*elasticBeamColumn*) with parameters like cross-sectional area, elastic modulus, shear modulus, moment of inertia, and torsional constant were used. The grillage-beam technique, chosen for its simplicity and accuracy over 3D finite-element models, represented the superstructure as interconnected beams. The torsional constants of the beam elements were reduced by half, assuming no interaction between axial force and bending moment in perpendicular directions. To account for the cracking effects, deck and girder elements had 40% of their sectional rigidity. Additionally, rigid connections (*rigidLink beams*) were assigned among the cap beam, girder, and deck elements to maintain structural continuity. At each end of the superstructure, roller support was defined to mimic the behavior of a seat-type abutment after shear-key failure.

The column displacement ductility capacity was 5.01 using the moment-curvature (M-ϕ) relationship obtained from OpenSees. The bridge system displacement ductility capacity was determined using OpenSees by the transverse displacement-controlled pushover analysis, which involved applying reference horizontal loads at the center of the pier caps with a target displacement level set at a 10% drift ratio. The results indicated a displacement ductility capacity of 10.0, with the column drift ratio at failure identified at 9.3%. The first vibration mode of the bridge was a rotational mode with a period of 1.31 seconds. The second and third modes represented transverse and longitudinal modes, each with a period of 1.0 second. The fourth mode corresponded to symmetric-bending modes with a period of 0.18 seconds. Figure 5 illustrates the mode shapes of the 3D bridge model, utilizing mass and last committed stiffness proportional Rayleigh damping. A 5% damping ratio was applied to the 1st and 3rd

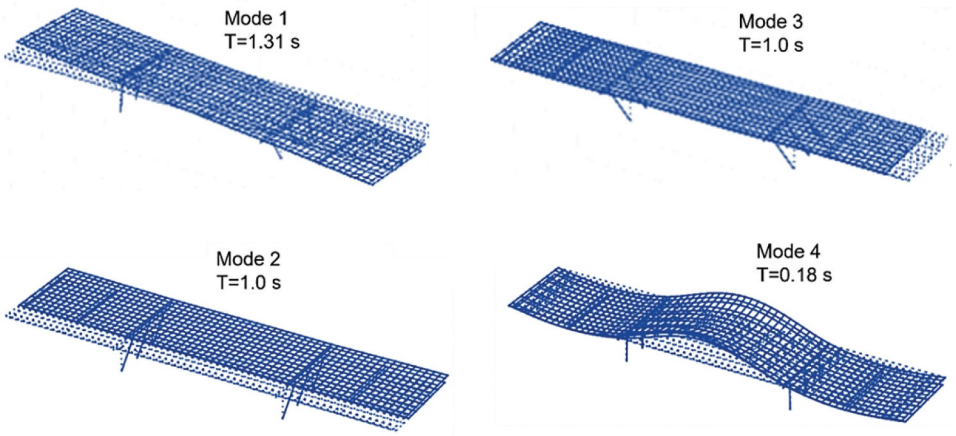

Figure 5. The first four mode shapes of the bridge model.

modes. Our observations indicated that the symmetric design of the bridge and equal stiffness of the bents led to almost zero in-plane rotation. This was determined by calculating the ratio of the difference between abutment transverse displacements (obtained from NRHA) to the bridge length. The near-zero in-plane rotation indicated that the rotational mode of the bridge (i.e. the first mode) was not activated.

5. Distribution of Structural Response Parameters

The column drift ratio (CDR), transverse displacement ductility demand (μ_D), and residual drift ratio (RDR) were considered as structural response parameters. CDR was calculated by taking the ratio of the maximum transverse displacement at the top of the column to the column height. μ_D was determined by calculating the ratio between the maximum displacement at the top of the column and the yield displacement obtained from static pushover analysis. RDR was computed by dividing the permanent transverse displacement at the top of the column by the column height.

Figures 6–8 depict cumulative distribution functions (CDFs) for CDR, μ_D, and RDR using elastic PSHA-based and inelastic PSHA-based GMSS approaches across three sites at $T_R = 975$ and 2475 years. In high-seismicity sites like Los Angeles and San Bernardino, elastic PSHA-based UHS ground motions resulted in comparable or slightly higher mean and dispersion values in CDR and μ_D compared to the inelastic PSHA-based motions at $T_R = 975$ years. In contrast, for lower seismicity site, i.e. San Francisco, both GMSS approaches yielded similar results. At $T_R = 2475$ years, the average μ_D in San Bernardino was around 5, while in Los Angeles, it ranged between 2.5 and 3.0. It was observed that the inelastic PSHA-based GMSS approach reduced the dispersion in CDR and μ_D for the highest seismicity site, i.e. San Bernardino, compared to the elastic PSHA-based GMSS. However, in Los Angeles, both GMSS approaches typically generated similar results, albeit with a slight underestimation in elastic PSHA-based motions.

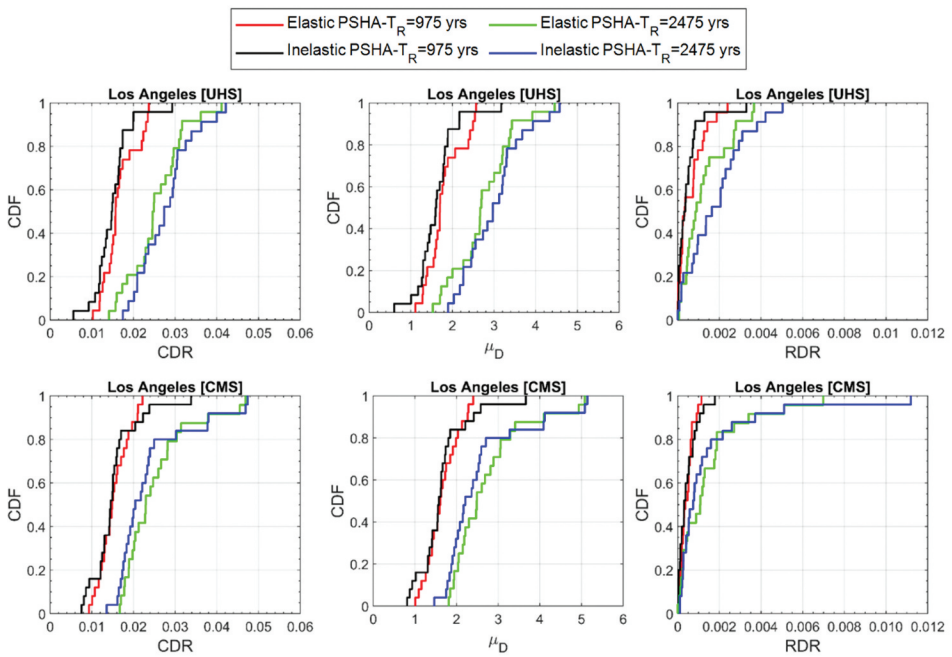

Figure 6. CDFs of CDR, μ_D, and RDR obtained from elastic PSHA- and inelastic PSHA-based GMSS approaches at $T_R = 975$ and 2475 years in Los Angeles.

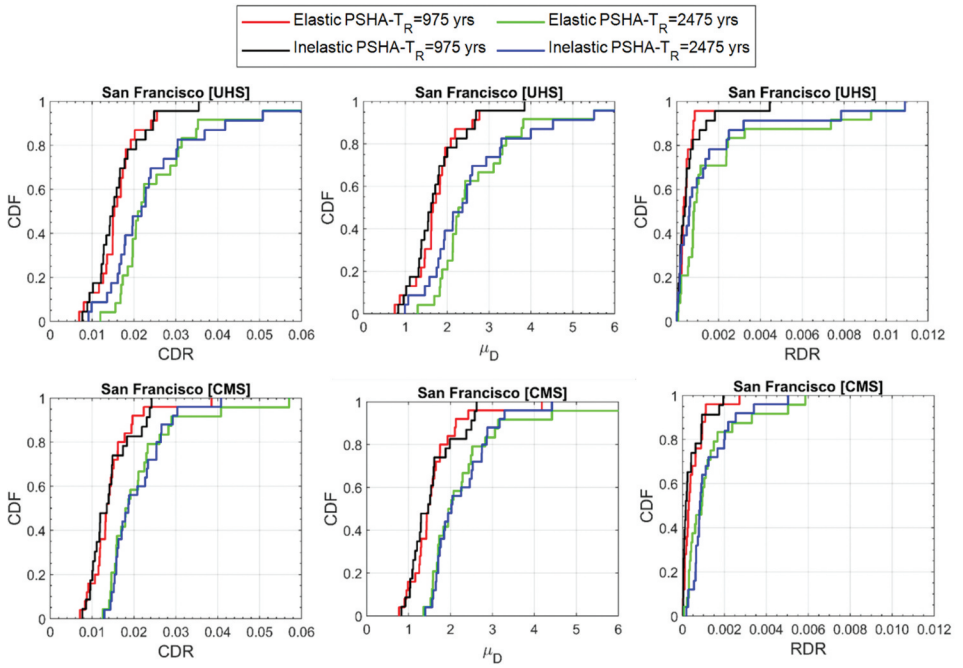

Figure 7. CDFs of CDR, μ_D, and RDR obtained from elastic PSHA and inelastic PSHA-based GMSS approaches at $T_R = 975$ years and $T_R = 2475$ years in San Francisco.

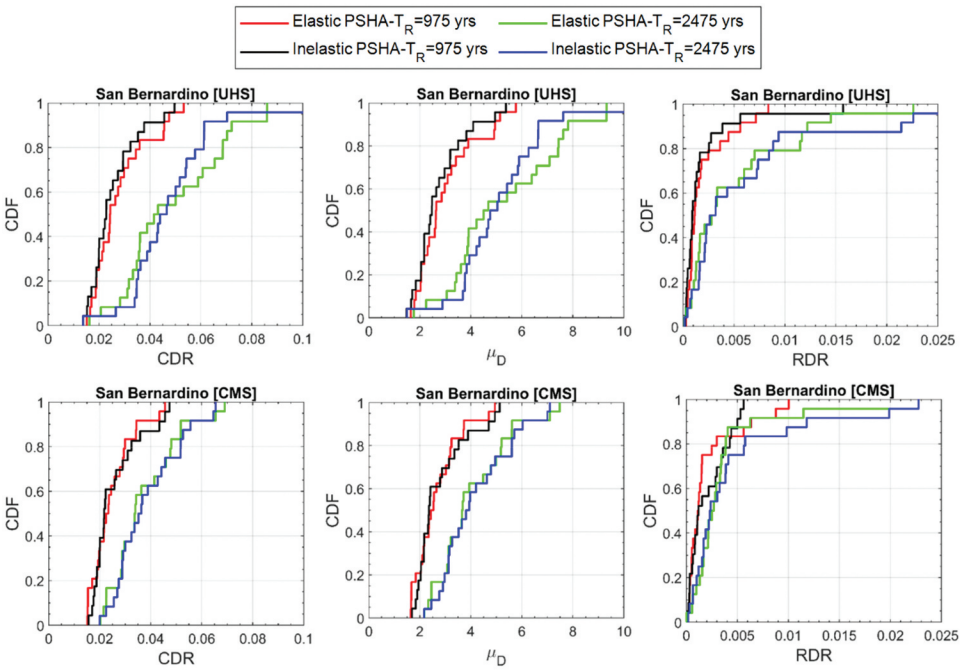

Figure 8. CDFs of CDR, μ_D, and RDR obtained from elastic PSHA and inelastic PSHA-based GMSS approaches at $T_R = 975$ years and $T_R = 2475$ years in San Bernardino.

For target CMS, ground motions selected by different GMSS approaches produced comparable distributions of CDR and μ_D for both return periods. This resulted from the good agreement between the mean spectra of elastic PSHA-based motions and the target inelastic spectra across various ductility levels for the specified T_R levels. While these results offer insights into the behavior of the bridge at two T_R levels, a more comprehensive analysis, particularly for fragility curve estimations, should consider multiple return periods. In comparing CMS and UHS cases, CMS-based motions produced lower mean structural responses, particularly at higher seismic hazard levels (e.g. $T_R = 2475$ years). This is expected since UHS, representing multiple scenarios, tends to produce higher spectral accelerations and, consequently, more conservative mean response estimates.

For RDRs, the mean values for Los Angeles and San Francisco remained below 0.2% at $T_R = 975$ and 2475 years. However, for the high-seismicity San Bernardino site, mean RDRs reached approximately 0.21% at $T_R = 975$ years and 0.6% at $T_R = 2475$ years. Although mean RDRs were below the 1% post-earthquake serviceability limit set by some design codes like Japan (JSCE 2000), large dispersions, observed in the upper tails of the CDF plots, led to the 1% RDR being exceeded in sites with high seismicity. The high variability observed in RDRs compared to CDR and μ_D suggests that RDRs are more sensitive to the specific characteristics of the ground motions, particularly in high-seismicity areas. The findings indicate that pulse characteristics could be one of the key factors affecting the response, as discussed in the following section.

Welch's t-test was employed to assess whether the differences between the means from two different GMSS approaches were statistically significant. This test facilitates the comparison of means from different samples without assuming equal variances (Welch 1947). The results revealed that the mean differences in response metrics between the two methods were not statistically significant at the chosen significance level ($p > 0.05$). While this finding suggests that the inelastic PSHA-based GMSS method and the traditional elastic PSHA-based method produce statistically similar results, the analysis aimed to assess not just statistical significance but also the broader trends and effectiveness of the proposed GMSS approach. Despite the lack of statistically significant differences, the proposed GMSS method shows efficacy in reducing response variability and improving the consistency of bridge response predictions, particularly in high seismic zones. The following sections of the paper provide further insight into these aspects.

5.1. Sensitivity of Residual Drift to Pulse Records

The comparisons between T_p and RDR for pulse records from elastic and inelastic PSHA-based GMSS approaches in San Bernardino at $T_R = 2475$ years are presented in Fig. 9. The plots also show average

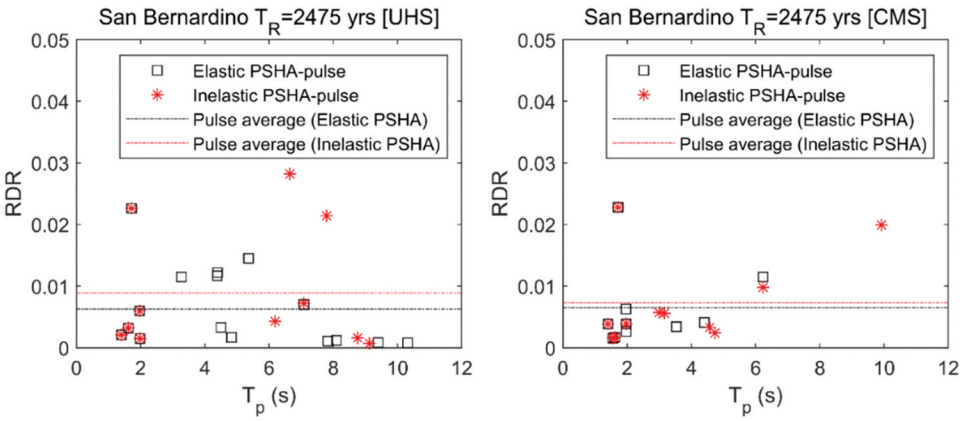

Figure 9. Comparisons of pulse period (T_p) and residual drift ratio (RDR) for elastic and inelastic PSHA-based GMSS approaches in San Bernardino at $T_R = 2475$ years.

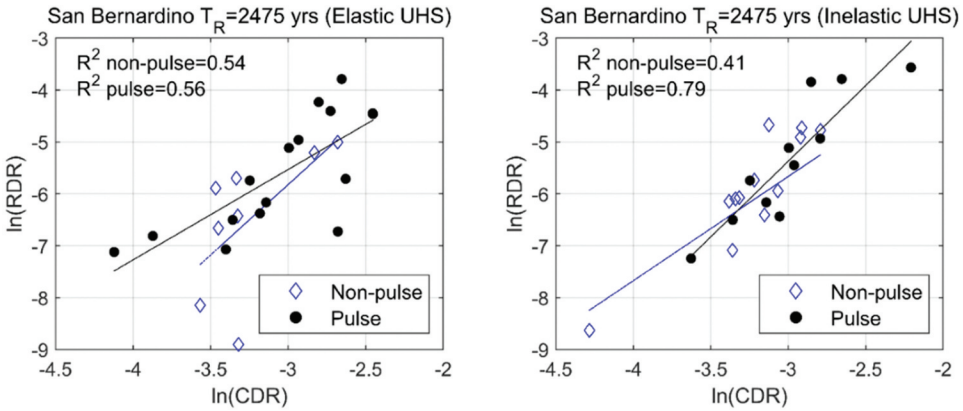

Figure 10. Relationships between natural logarithms of CDRs and RDRs obtained from pulses and non-pulses using elastic and inelastic UHS-based GMSS approaches in San Bernardino at $T_R = 2475$ years.

RDRs from pulses, considering all pulse-like ground motions within the pool of 25 motions. The San Bernardino case was chosen because both GMSS approaches included more than ten pulses, allowing for meaningful statistical interference. It was observed that the UHS-based subsets had a higher number of pulses compared to CMS-based subsets. The results indicated that, on average, pulses produced higher RDRs than pooled motions, as shown in the CDF plot in Fig. 8. For instance, elastic UHS motions had pooled RDRs of 0.51%, while pulse RDRs reached 0.63%. Similarly, in the case of inelastic UHS motions, pooled RDRs were 0.62%, and pulses resulted in 0.82%. These observations were consistent with the results of the shake table test (H. Choi et al. 2010; Phan et al. 2007). The results also demonstrated that pulses with $T_p > 3T_1$ could yield RDRs exceeding 1%. This suggests that T_p values not coinciding with the elongated period of the structure could still result in significant structural responses, which can be attributed to the amplitude of the pulses. These findings highlight the need to account for pulse effects and RDRs in seismic design to improve bridge resilience post-earthquake (Zengin et al. 2025).

To understand the effect of the distribution of CDRs on RDRs, the relationships between the natural logarithms of CDRs and RDRs are illustrated in Fig. 10. The plots include both pulses and non-pulses obtained from UHS-based GMSS approaches in San Bernardino at $T_R = 2475$ years. The linear regression fitted to the data points, along with the corresponding coefficient of determination (R^2) values, are also shown. The positive trends and relatively strong correlation between pulse CDRs and RDRs suggested that pulses tended to produce higher CDRs than non-pulses, leading to higher RDRs. The findings revealed that while a GMSS approach can reduce dispersion in CDRs, it may not reduce dispersion in RDRs, especially with pulse records.

6. Probabilistic Seismic Performance and Risk Assessment

Fragility curves, crucial in earthquake engineering for assessing structural vulnerability, have been developed through analyzing diverse data sources, including experimental, numerical, and field data (E. Choi, DesRoches, and Nielson 2004; Padgett and DesRoches 2008; Vosooghi and Saiidi 2012). These curves estimate the conditional probabilities of EDPs exceeding predefined damage limit states at different seismic hazard levels. Previous studies employed various EDPs, such as column-curvature ductility, drift ratio, RDR, yielding of reinforcement, and abutment deformation for probabilistic seismic bridge assessment (Mackie and Stojadinović 2001; Muntasir Billah and Alam 2015; Padgett and DesRoches 2008; Ramanathan, DesRoches, and Padgett 2012). In this study, the seismic performance of the three-span bridge was evaluated based on CDR. For the bridge damage states (DSs), experimental fragility curves defined by Vosooghi and Saiidi (2012) were adopted as the capacity-

Table 2. Definitions of the damage states.

DSi	Definitions
DS_1	Flexural cracks
DS_2	Minor spalling and possible shear cracks
DS_3	Extensive cracks and spalling
DS_4	Visible lateral and/or longitudinal reinforcing bars; and
DS_5	Compressive failure of the concrete core edge (imminent failure)
DS_6	Failure

Table 3. Median and logarithmic standard deviation values of CDR-based DS fragility curves.

	DS_1	DS_2	DS_3	DS_4	DS_5
S_c	0.0165	0.028	0.043	0.060	0.079
β_c	0.425	0.332	0.264	0.303	0.353

based limit state model. Their work was based on data from 32 bridge columns, primarily tested on shake tables, and resulted in fragility curves for six EDPs corresponding to six damage states (DSs). These DSs ranged from flexural cracks (DS_1) to failure (DS_6). The six different EDPs considered were the maximum drift ratio (MDR), RDR, frequency ratio (FR), inelasticity index (II), maximum longitudinal steel strain (MLS), and maximum transverse steel strain (MTS). These damage states were defined based on the severity of damage observed in the columns of the bridge. Table 2 provides the definitions of all DSs. Table 3 lists the median (S_c) and logarithmic standard deviation (β_c) values of CDR-based DS fragility curves.

6.1. Probability of Exceedances of Damage States

The probability that the demand is exceeding the capacity (see Table 3) for a given IM level (Nielson 2005) can be expressed as follows:

$$P[D > C|IM] = \Phi\left[\frac{\ln\left(\frac{S_d}{S_c}\right)}{\sqrt{\beta_{D|IM}^2 + \beta_c^2}}\right] \tag{1}$$

where Φ denotes the cumulative standard normal distribution, S_d is the mean estimate of the demand, $\beta_{D|IM}$ corresponds to the logarithmic standard deviations of the demand. The total uncertainty is the square root of the sum of the squares of these standard deviations.

The probabilities of CDR exceeding DS thresholds (P(CDR>DS_i)) at T_R = 975 years and T_R = 2475 years were depicted in Fig. 11 for each site. At T_R = 975 years, the elastic PSHA-based GMSS approach, using UHS, generally resulted in more conservative DS exceedance probabilities, especially at high-seismicity sites. In contrast, the inelastic PSHA-based GMSS approach provided less conservative estimates. For CMS-based ground motions at T_R = 975 years, the elastic PSHA-based approach resulted in slightly lower mean and dispersion in structural responses, which led to lower DS exceedance probabilities compared to the inelastic approach.

At T_R = 2475 years, the inelastic PSHA-based GMSS approach often produced DS exceedance probabilities that were similar to or slightly higher than those from the elastic PSHA-based GMSS, especially at higher DS. This difference is influenced by how demand and capacity distributions interact. Except for San Bernardino, the elastic PSHA-based approach generally provided comparable or slightly higher exceedance probabilities than the inelastic approach. Comparing UHS- and CMS-based cases, CMS-based ground motions from both GMSS approaches led to lower DS exceedance probabilities, especially for DS_3 levels at T_R = 2475 years.

The findings indicate that at T_R = 975 years, the three-span bridge is prone to flexural cracks in Los Angeles and San Francisco, with potential minor spalling and shear cracks in San Bernardino. At T_R =

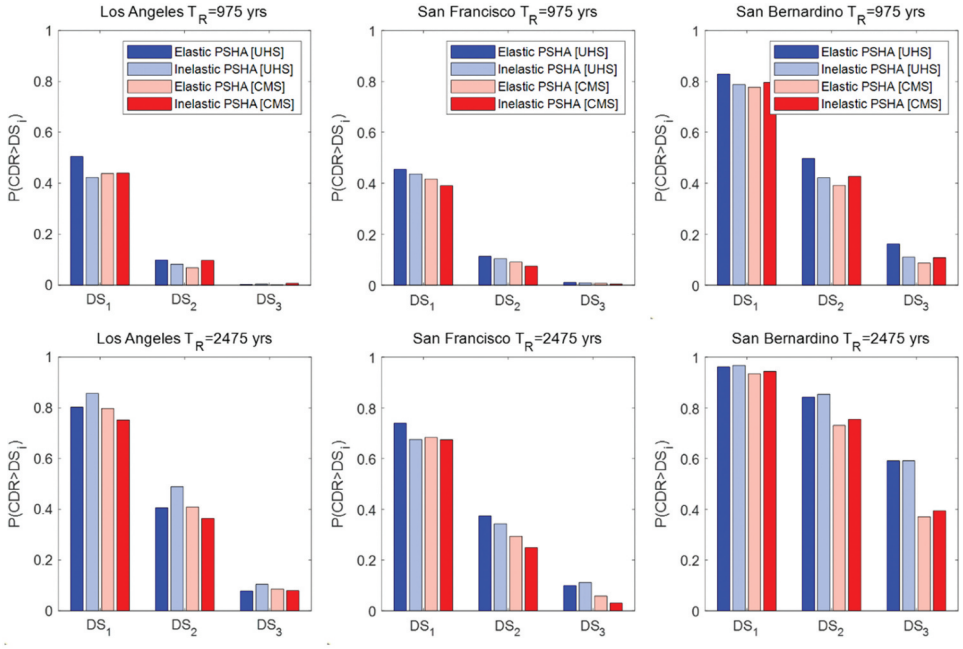

Figure 11. The probabilities of CDR exceeding DS thresholds at $T_R = 975$ years and $T_R = 2475$ years.

2475 years, the bridge is more likely to experience minor spalling and shear cracks in Los Angeles and San Francisco, while extensive cracks and spalling may occur in San Bernardino. Saini and Saiidi (2014) associated DSs with bridge functionality. At DS_1, the bridge remains fully operational with no repairs. DS_2 may not impact functionality but requires repairs at plastic hinge locations. DS_3 leads to closure and repairs for the entire column. Damage severity and required repairs would increase with higher DS levels.

6.2. Analytical Fragility Curves

By utilizing discrete probabilities computed from Eq. 1 at five T_R levels, the lognormal distribution was fitted to these probabilities through minimizing the SSE between the actual and fitted values. Figure 12 depicts fragility curves derived from UHS-based ground motions with different GMSS approaches (left panel) and CMS-based ground motions (right panel). San Bernardino fragility functions had three DSs; for other sites, curves included only DS_1 and DS_2 because DS_3 threshold exceedances were observed in a limited number of instances. Tables 4 and 5 list the median Sa (θ) and the logarithmic standard deviation values (β) of the UHS-and CMS-based fragility curves for each site, respectively. The θ represents a 50% probability of exceeding a specific DS level. A higher θ value implies that the bridge can withstand earthquakes of higher intensity. The β dictates the slope of the fragility curve. Reduced dispersion results in steeper curves, typically indicating a decrease in exceedance probabilities at lower Sa levels and an increase at higher Sa levels.

The results revealed that inelastic UHS-based motions generally resulted in comparable or reduced dispersion in fragility curves compared to elastic UHS-based motions, with some exceptions. The inelastic PSHA-based GMSS approach typically reduced conservatism observed with the elastic PSHA-based approach. However, when evaluating CMS-based fragilities, the impact of GMSS approaches on conservatism and dispersion varied by site and was not consistent. Generally, UHS-based fragility curves showed lower θ values than CMS-based counterparts, indicating increased vulnerability, especially at higher DS levels. The fragility curves derived considering only demand

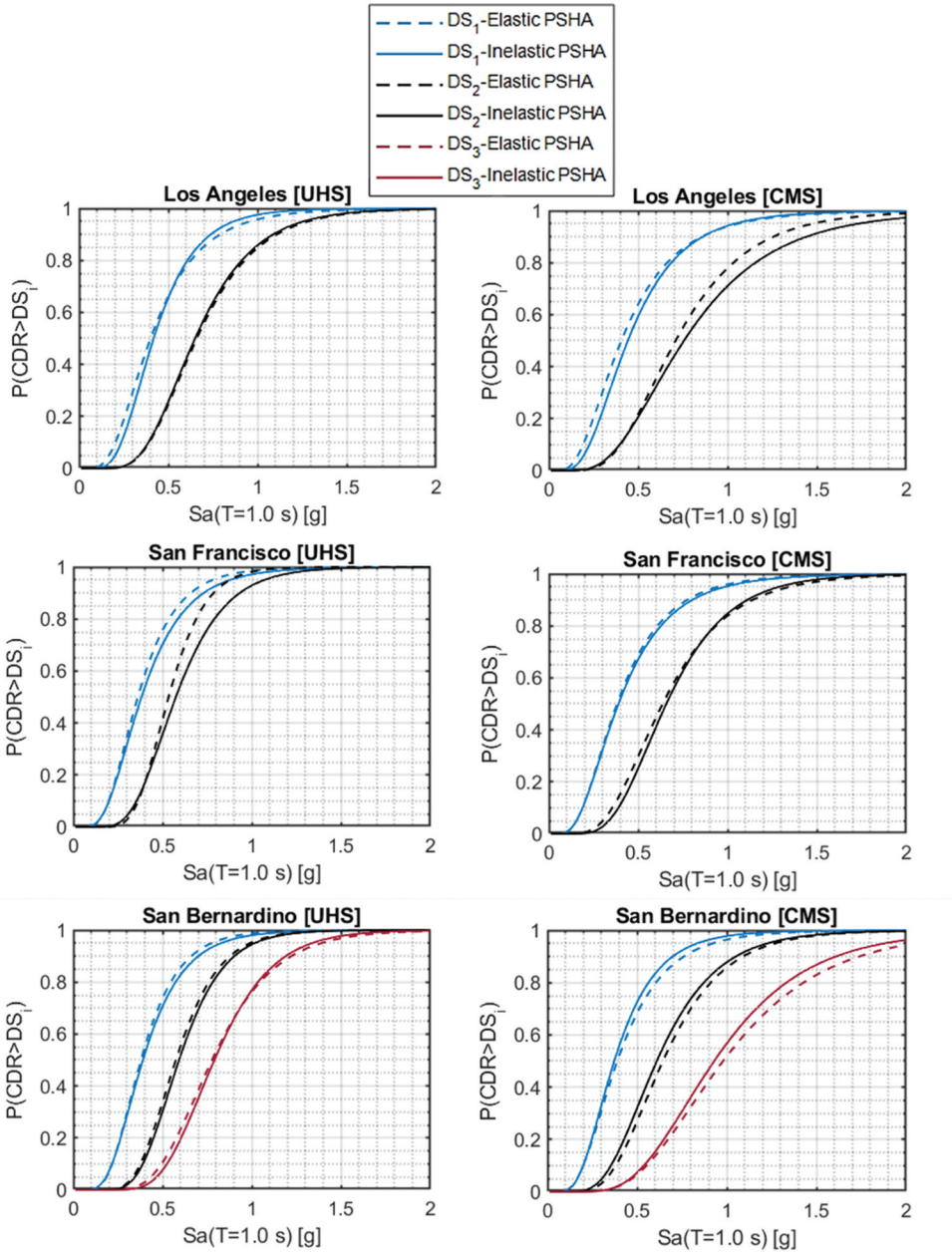

Figure 12. Fragility curves including demand and capacity uncertainties for different GMSS approaches.

Table 4. Parameters of UHS-based fragility curves including demand and capacity uncertainties.

	DS_1-Elastic PSHA		DS_1-Inelastic PSHA		DS_2-Elastic PSHA		DS_2-Inelastic PSHA		DS_3-Elastic PSHA		DS_3- Inelastic PSHA	
Site	θ	β	θ	β	θ	β	θ	β	θ	β	θ	β
Los Angeles	0.40	0.53	0.42	0.44	0.66	0.40	0.65	0.40	–	–	–	–
San Francisco	0.36	0.47	0.38	0.51	0.53	0.30	0.57	0.38	–	–	–	–
San Bernardino	0.38	0.43	0.39	0.46	0.57	0.33	0.59	0.33	0.78	0.35	0.79	0.32

Table 5. Parameters of CMS-based fragility curves including demand and capacity uncertainties.

	DS_1-Elastic PSHA		DS_1-Inelastic PSHA		DS_2-Elastic PSHA		DS_2-Inelastic PSHA		DS_3-Elastic PSHA		DS_3- Inelastic PSHA	
Site	θ	β	θ	β	θ	β	θ	β	θ	β	θ	β
Los Angeles	0.41	0.58	0.44	0.52	0.71	0.45	0.76	0.51	–	–	–	–
San Francisco	0.38	0.55	0.39	0.56	0.64	0.46	0.66	0.41	–	–	–	–
San Bernardino	0.39	0.52	0.37	0.49	0.64	0.41	0.61	0.42	0.98	0.45	0.93	0.43

uncertainty showed similar differences between GMSS approaches. Excluding capacity uncertainties slightly reduced vulnerability (shifted curves rightward) and decreased dispersion of the fragility curve (Zengin, Saiidi, and Bozorgnia 2023).

6.3. Seismic Risk Curves

The seismic risk curve, or EDP hazard curve, results from convolving the fragility curve with the mean seismic hazard curve. The annual rate of exceedance for a CDR threshold level ($\lambda_{CDR}(x)$), namely the seismic risk curve, can be computed using Equation 2 (Kiureghian 2005; Krawinkler and Miranda 2004). This study employs a discrete summation approximation to calculate the annual rate of exceedance for a specified CDR threshold level x.

$$\lambda_{CDR}(x) = \sum_{im_i} P(CDR > x | IM = im_i).\Delta\lambda_{IM}(im_i) \quad (2)$$

where $P(CDR > x|IM = im_i)$ corresponds the probability of exceeding a specified CDR level, x, for a given $IM = im_i$. $\Delta\lambda_{IM}(im_i) = \lambda_{IM}(im_i) - \lambda_{IM}(im_{i+1})$ denotes the approximation for the annual rate of occurrence of IM being equal to im_i. The CDR responses were derived from distinct sets of scaled ground motions for each target IM level. It was assumed that the structural response at each IM (or T_R level) followed a lognormal distribution.

Figure 13 compares CDR risk curves for the bridge across different GMSS approaches at each site. When using UHS as a target, it was observed that the elastic PSHA-based GMSS approach produced slightly higher or comparable annual rates of exceedances of CDR compared to the inelastic PSHA-based GMSS approach. When using CMS as a target, the elastic PSHA-based GMSS produced slightly unconservative results compared to the inelastic GMSS approach in the site with the highest seismicity, namely San Bernardino, while opposite patterns were observed in Los Angeles and San Francisco. These observations validated the trend noted in the fragility curves. However, the differences were generally not substantial, given that the fragility curves for the three-span bridge used in this study were closely aligned.

The results indicated that the differences in seismic risk curves were affected by the chosen target spectra definitions, namely UHS and CMS, especially at higher CDR levels (i.e. CDR > 0.03). CDR curves from CMS-based motions typically demonstrated a lower bound (in terms of both annual probability of exceedance and CDR) compared to UHS-based motions. This suggests that the UHS-based approach is generally more conservative in assessing seismic risk, leading to a higher annual rate of exceeding a CDR level.

7. Conclusions

This study assessed the impact of two GMSS approaches, one utilizing traditional elastic PSHA-based target spectra and the other using inelastic PSHA-based target spectra with various ductility levels, on the seismic responses of a three-span, three-column bent, typical bridge designed according to Caltrans SDC. The investigation focused on five California sites with different seismicity, three of which are presented in this article due to limited space: Los Angeles, San Francisco, and San Bernardino. Comparing the column drift ratio (CDR), displacement ductility (μ_D), and residual

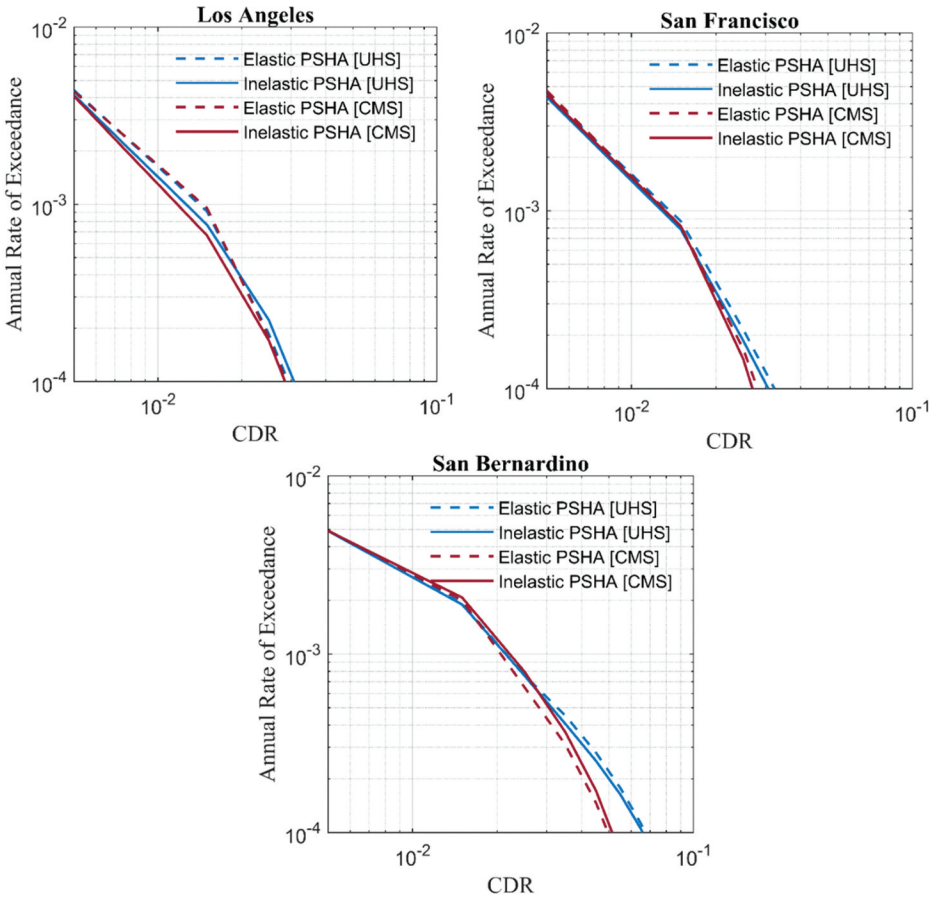

Figure 13. Comparisons of CDR risk curves based on different GMSS approaches. The solid line corresponds to the inelastic PSHA-based GMSS approach, and the dashed line depicts the elastic PSHA-based GMSS approach.

drift ratio (RDR) at return periods (T_R) of 975 and 2475 years revealed that using elastic PSHA-based UHS motions led to responses comparable to, and somewhat higher than, those obtained using inelastic PSHA-based motions at $T_R = 975$ years. At $T_R = 2475$ years, the inelastic PSHA-based UHS motions tended to reduce the dispersion in structural response compared to the elastic PSHA-based UHS motions, especially in the site with the highest seismicity (San Bernardino). Using CMS as a target, both GMSS approaches yielded comparable mean CDR and μ_D responses, attributed to the inelastic spectra of ground motions selected based on the elastic approach showing good agreement with the target inelastic spectra across various ductility levels. The findings also indicated that the RDRs were significantly affected by the characteristics of the pulse motions, highlighting the importance of considering these effects in seismic design of bridges.

The results showed that fragility curves based on CDR derived from inelastic PSHA-based UHS generally slightly reduced the dispersion, particularly in the highest seismicity site, San Bernardino, enabling more accurate estimation. Seismic risk curves followed similar patterns as observed in fragility curves. Generally, elastic UHS motions resulted in comparable or slightly higher (i.e. conservative) annual rates of CDR exceedances compared to inelastic UHS motions. The level of conservatism in the elastic CMS-based fragilities and risk curves varied, depending on the degree of mismatch between recorded and target inelastic spectra. The reduced dispersion from the inelastic PSHA-based UHS makes this method attractive when

designers try to avoid unnecessary conservatism associated with the elastic UHS motions. Comparisons of seismic risk curves highlighted the significant impact of selected target spectra, UHS and CMS, especially at higher CDR levels exceeding 3%. In particular, the CMS-based risk curves tended to yield lower annual rates of exceedances than the UHS-based counterparts.

The findings of this study revealed differences between the GMSS approaches, with implications for fragility curves and risk curves, emphasizing the need for careful selection of GMSS approaches and target spectra when assessing seismic performance and risk of bridges. The study also highlighted the potential benefits of recent developments in inelastic PSHA-based target spectra and GMSS approach for reducing dispersion in structural responses, especially in high seismicity sites. The expense of such an advantage is a somewhat more complex analysis of seismic hazard using inelastic target spectra. The use of inelastic PSHA-based target spectra may be justified in special cases when a higher degree of certainty is desired.

The fragility functions and seismic risk curves in this study are tailored to the simple representative bridge configurations, seismic hazard levels, and assumed boundary conditions, providing a foundation for future 3D multi-component analyses. Future research should also address uncertainties such as geometry, material properties, various bridge types, and the number of ground motions.

Acknowledgments

The authors would like to express their sincere gratitude to Dr. Elmira Shoushtari for her support in OpenSees bridge modeling. Additionally, special thanks to Dr. Amarjeet Saini for generously providing the experimental fragility curve data used in this study.

Disclosure Statement

No potential conflict of interest was reported by the author(s).

Funding

This study was supported by the California Department of Transportation (Caltrans) and coordinated by the Natural Hazards Risk and Resiliency Research Center (NHR3) headquartered at UCLA. The support is gratefully acknowledged. The findings, conclusions, or recommendations in this publication are those of the authors and do not necessarily represent those of the sponsors.

Data Availability Statement

The data that support the findings of this study are available from the corresponding author upon reasonable request.

References

Aviram, A., K. R. Mackie, and B. Stojadinovic. 2008. "Effect of Abutment Modeling on the Seismic Response of Bridge Structures." *Earthquake Engineering and Engineering Vibration* 7 (4): 395–402. https://doi.org/10.1007/s11803-008-1008-3.

Bahrampouri, M., Y. Bozorgnia, S. Mazzoni, and K. Campbell. 2023. "Use of Inelastic Response Spectra in Seismic Hazard Analysis and Design." https://doi.org/10.34948/N38G6K;.

Baker, J. W. 2011. "Conditional Mean Spectrum: Tool for Ground-Motion Selection." *Journal of Structural Engineering* 137 (3): 322–331. https://doi.org/10.1061/(ASCE)ST.1943-541X.0000215.

Boore, D. M. 2010. "Orientation-Independent, Non Geometric-Mean Measures of Seismic Intensity from Two Horizontal Components of Motion." *Bulletin of the Seismological Society of America* 100 (4): 1830–1835. https://doi.org/10.1785/0120090400.

Bozorgnia, Y., N. A. Abrahamson, L. Al Atik, T. D. Ancheta, G. M. Atkinson, J. W. Baker, A. Baltay, et al. 2014. "NGA-West2 Research Project." *Earthquake Spectra* 30 (3): 973–987. https://doi.org/10.1193/072113EQS209M.

Bozorgnia, Y., and V. V. Bertero. 2004. *Earthquake Engineering: From Engineering Seismology to Performance-Based Engineering*. Boca Raton, FL: CRC Press.
Bozorgnia, Y., M. M. Hachem, and K. W. Campbell. 2010. "Ground Motion Prediction Equation ("Attenuation Relationship") for Inelastic Response Spectra." *Earthquake Spectra* 26 (1): 1–23. https://doi.org/10.1193/1.3281182.
Bradley, B. 2010. "A Generalized Conditional Intensity Measure Approach and Holistic Ground-Motion Selection." *Earthquake Engineering & Structural Dynamics* 39 (12): 1321–1342. https://doi.org/10.1002/eqe.995.
Campbell, K. W., and Y. Bozorgnia. 2014. "NGA-West2 Ground Motion Model for the Average Horizontal Components of PGA, PGV, and 5% Damped Linear Acceleration Response Spectra." *Earthquake Spectra* 30 (3): 1087–1115. https://doi.org/10.1193/062913EQS175M.
Choi, E., R. DesRoches, and B. Nielson. 2004. "Seismic Fragility of Typical Bridges in Moderate Seismic Zones." *Engineering Structures* 26 (2): 187–199. https://doi.org/10.1016/j.engstruct.2003.09.006.
Choi, H., M. S. Saiidi, P. Somerville, and S. El-Azazy. 2010. "Experimental Study of Reinforced Concrete Bridge Columns Subjected to Near-Fault Ground Motions." *ACI Structural Journal* 107 (1): 3.
Field, E. H., R. J. Arrowsmith, G. P. Biasi, P. Bird, T. E. Dawson, K. R. Felzer, and Y. Zeng. 2014. "Uniform California Earthquake Rupture Forecast, Version 3 (UCERF3)—The Time-Independent Model." *Bulletin of the Seismological Society of America* 104 (3): 1122–1180. https://doi.org/10.1785/0120130164.
Jayaram, N., T. Lin, and J. W. Baker. 2011. "A Computationally Efficient Ground-Motion Selection Algorithm for Matching a Target Response Spectrum Mean and Variance." *Earthquake Spectra* 27 (3): 797–815. https://doi.org/10.1193/1.3608002.
JSCE. 2000. *Earthquake Resistant Design Codes in Japan*. Tokyo, Japan: Japan Society of Civil Engineers, Earthquake Engineering Committee.
Kiureghian, A. D. 2005. "Non-Ergodicity and PEER's Framework Formula." *Earthquake Engineering & Structural Dynamics* 34 (13): 1643–1652. https://doi.org/10.1002/eqe.504.
Kohrangi, M., P. Bazzurro, and D. Vamvatsikos. 2016. "Vector and Scalar IMs in Structural Response Estimation, Part I: Hazard Analysis." *Earthquake Spectra* 32 (3): 1507–1524. https://doi.org/10.1193/053115EQS080M.
Krawinkler, H., and E. Miranda. 2004. *Performance-Based Earthquake Engineering. Earthquake Engineering: From Engineering Seismology to Performance-Based Engineering, Bozorgnia and Bertero (Ed.)*. Boca Raton, FL: CRC Press.
Kullback, S., and R. A. Leibler. 1951. "On Information and Sufficiency." *Annals of Mathematical Statistics* 22 (1): 79–86. https://doi.org/10.1214/aoms/1177729694.
Mackie, K., and B. Stojadinović. 2001. "Probabilistic Seismic Demand Model for California Highway Bridges." *Journal of Bridge Engineering* 6 (6): 468–481. https://doi.org/10.1061/(ASCE)1084-0702(2001)6:6(468).
Mander, J. B., M. J. N. Priestley, and R. Park. 1988. "Observed Stress-Strain Behavior of Confined Concrete." *Journal of Structural Engineering* 114 (8): 1827–1849. https://doi.org/10.1061/(ASCE)0733-9445(1988)114:8(1827).
Mazzoni, S., F. McKenna, M. H. Scott, and G. L. Fenves. 2006. "OpenSees Command Language Manual." *Pacific Earthquake Engineering Research (PEER) Center* 264 (1): 137–158.
Mazzoni, S., Y. Bozorgnia, and M. Bahrampouri. 2023. "Expansion of NGA-West2 Ground-Motion Database to Include Inelastic-Response Intensity Measures." *GIRS 2023-07 Report*. https://doi.org/10.34948/N3B88W.
McKenna, F., M. H. Scott, and G. L. Fenves. 2010. "Nonlinear Finite-Element Analysis Software Architecture Using Object Composition." *Journal of Computing in Civil Engineering* 24 (1): 95–107. https://doi.org/10.1061/(ASCE)CP.1943-5487.0000002.
Menegotto, M., and P. Pinto. 1973. "Method of Analysis for Cyclically Loaded Reinforced Concrete Plane Frames Including Changes in Geometry and Non-elastic Behavior of Elements Under Combined Normal Force and Bending." In Proceedings IABSE, Symposium on the Resistance and Ultimate Deformability of Struct. Acted on by Well-Defined Repeated Loads. Vol. 13. Lisbon, Portugal: IABSE Reports.
Monteiro, R., C. Zelaschi, A. Silva, and R. Pinho. 2019. "Derivation of Fragility Functions for Seismic Assessment of RC Bridge Portfolios Using Different Intensity Measures." *Journal of Earthquake Engineering* 23 (10): 1678–1694. https://doi.org/10.1080/13632469.2017.1387188.
Muntasir Billah, A. H. M., and M. S. Alam. 2015. "Seismic Fragility Assessment of Concrete Bridge Pier Reinforced with Superelastic Shape Memory Alloy." *Earthquake Spectra* 31 (3): 1515–1541. https://doi.org/10.1193/112512EQS337M.
Neuenhofer, A., and F. C. Filippou. 1998. "Geometrically Nonlinear Flexibility-Based Frame Finite Element." *Journal of Structural Engineering* 124 (6): 704–711. https://doi.org/10.1061/(ASCE)0733-9445(1998)124:6(704).
Nielson, B. G. 2005. "*Analytical Fragility Curves for Highway Bridges in Moderate Seismic Zones*." Ph.D. thesis, Atlanta: Georgia Institute of Technology.
Padgett, J. E., and R. DesRoches. 2008. "Methodology for the Development of Analytical Fragility Curves for Retrofitted Bridges." *Earthquake Engineering & Structural Dynamics* 37 (8): 1157–1174. https://doi.org/10.1002/eqe.801.
Phan, V., M. S. Saiidi, J. Anderson, and H. Ghasemi. 2007. "Near-Fault Ground Motion Effects on Reinforced Concrete Bridge Columns." *Journal of Structural Engineering* 133 (7): 982–989. https://doi.org/10.1061/(ASCE)0733-9445(2007)133:7(982).
Ramanathan, K., R. DesRoches, and J. E. Padgett. 2012. "A Comparison of Pre-And Post-Seismic Design Considerations in Moderate Seismic Zones Through the Fragility Assessment of Multispan Bridge Classes." *Engineering Structures* 45:559–573. https://doi.org/10.1016/j.engstruct.2012.07.004.

Saini, A., and M. Saiidi. 2014. *Probabilistic Damage Control Approach for Seismic Design of Bridge Columns*. Sacramento, CA: California Department of Transportation.
Scott, M. H., and O. M. Hamutçuoğlu. 2008. "Numerically Consistent Regularization of Force-Based Frame Elements." *International Journal for Numerical Methods in Engineering* 76 (10): 1612–1631. https://doi.org/10.1002/nme.2386.
SDC. 2019. *Seismic Design Criteria Version 2.0*. Sacramento, CA: California Department of Transportation (Caltrans).
Shahi, S. K., and J. W. Baker. 2014. "An Efficient Algorithm to Identify Strong-Velocity Pulses in Multicomponent Ground Motions." *Bulletin of the Seismological Society of America* 104 (5): 2456–2466. https://doi.org/10.1785/0120130191.
Shoushtari, E., M. S. Saiidi, A. Itani, and M. A. Moustafa. 2021. "Seismic Performance of a Two-Span Steel Girder Bridge with ABC Connections." *Engineering Structures* 241:112502. https://doi.org/10.1016/j.engstruct.2021.112502.
Tarbali, K., B. A. Bradley, and J. W. Baker. 2019. "Ground Motion Selection in the Near-Fault Region Considering Directivity-Induced Pulse Effects." *Earthquake Spectra* 35 (2): 759–786. https://doi.org/10.1193/102517EQS223M.
Vosooghi, A., and M. S. Saiidi. 2012. "Experimental fragility curves for seismic response of reinforced concrete bridge columns." *ACI Structural Journal* 109 (6): 825.
Welch, B. L. 1947. "The Generalization Of 'student's' Problem When Several Different Population Varlances are Involved." *Biometrika* 34 (1–2): 28–35. https://doi.org/10.1093/biomet/34.1-2.28.
Yassin, M. H. M. 1994. *Nonlinear Analysis of Prestressed Concrete Structures Under Monotonic and Cyclic Loads*. Berkeley: University of California.
Zengin, E. 2022. "Effectiveness of Instantaneous Power in Predicting the Collapse Responses of Structures Under Pulse-Like Ground Motions." *Advances in Structural Engineering* 25 (8): 1806–1814. https://doi.org/10.1177/136943322210766.
Zengin, E., and N. Abrahamson. 2020. "Conditional Ground-Motion Model for Damaging Characteristics of Near-Fault Ground Motions Based on Instantaneous Power." *Bulletin of the Seismological Society of America* 110 (6): 2828–2842. https://doi.org/10.1785/0120200124.
Zengin, E., and N. A. Abrahamson. 2020. "A Vector-Valued Intensity Measure for Near-Fault Ground Motions." *Earthquake Engineering & Structural Dynamics* 49 (7): 716–734. https://doi.org/10.1002/eqe.3261.
Zengin, E., and N. A. Abrahamson. 2021. "A Procedure for Matching the Near-Fault Ground Motions Based on Spectral Accelerations and Instantaneous Power." *Earthquake Spectra* 37 (4): 2545–2561. https://doi.org/10.1177/87552930211014540.
Zengin, E., S. Saiidi, and Y. Bozorgnia. 2023. "Influence of Ground Motion Selection and Scaling Approaches on Seismic Performance Assessment of Bridges." *GIRS-2023-11*. https://doi.org/10.34948/N3Z30Q.
Zengin, E., Y. Bozorgnia, S. Mazzoni, and K. Campbell. 2025. "Residual Displacement Ground-Motion Model." *Soil Dynamics and Earthquake Engineering* 190:109121. https://doi.org/10.1016/j.soildyn.2024.109121.
Zengin, E., Y. Bozorgnia, A. Tamhidi, and S. Mazzoni. 2024. "Spatial Distribution of Damage Potential of the 2023 Pazarcik Turkey Earthquake Using Inelastic-Response Spectra of Recorded and Simulated Ground Motions." *Earthquake Spectra*. https://doi.org/10.1177/87552930241270609.